INSTITUTO SUPERIOR TÉCNICO
Universidade Técnica de Lisboa

Automatic System for Diagnosis of Skin Lesions Based on Dermoscopic Images

Luís Filipe Caeiro Margalho Guerra Rosado

Dissertation to obtain the Masters Degree in

Biomedical Engineering

Abstract

This work aims to develop a prototype capable of segmenting skin lesions in dermoscopy images and classify them based on visual characteristics, particularly in detecting melanomas and separate them from other lesions. This work took as starting point the ABCD rule, which is based on 4 visual features, and for which was developed algorithms to measure and quantify them.

The proposed model is divided into three distinct stages: 1) Segmentation: implementation of a segmentation algorithm of dermoscopy images in order to determine the border of the lesion, based on the analysis of peaks and valleys of the histogram. 2) Feature extraction: definition of the features to use (asymmetry, color, border and differential structures) and development of routines for their automatic detection. 3) Classification: development of methods for automatic classification of dermoscopic images. The images were classified through a supervised method (classification is made taking into account the image analysis by a specialist), using a thresholding method, a k-nearest neighbors classifier and a Support Vector Machines classification.

The prototype was implemented in MATLAB, and was used a database of 68 dermoscopic images, courtesy of Dr. Jorge Rozeira of Hospital Pedro Hispano.

Keywords: Dermoscopy, ABCD rule, Segmentation, Feature extraction, Classification.

1. Introduction

The skin cancer corresponds to about one third of all cancers detected each year in Portugal, affecting 1 in every 7 people throughout life. It is estimated that malignant melanoma accounts for only 8% of skin cancers detected, but is responsible for more than 70% of the deaths. Around 800 new cases per year are detected in Portugal [1].

Early diagnosis of melanoma is extremely important, since the success rates of curing skin cancer are very high if detected during the early stages of its development [2].

Dermoscopy is a non-invasive diagnostic technique for the in vivo observation of pigmented skin lesions, which uses optical magnification and liquid immersion or polarized lightning to achieve better visualization of surface and subsurface structures of the skin [3].

The diagnosis of skin lesions from dermoscopy images is quite problematic due to the complexity and variability of its structures [4]. To increase the clinical applicability of dermoscopy, several diagnostic algorithms have been proposed during the last decades, being the ABCD rule one of the methods which become more widely accepted by clinicians. The ABCD rule was proposed in 1994 by Stolz *et al.* [5] and is based on the analysis of four different criteria: asymmetry (A), border (B), color

(C) and differential structures (D). Each criteria is analyzed semi-quantitatively and multiplied by a given weight factor in order to obtain the Total Dermoscopy Score (TDS). For more details see table 1.

Table 1 – The ABCD rule criterion [6].

Criteria	Description	Score	Weight factor
Asymmetry	In 0, 1, or 2 axes; assess not only contour, but also colors and structures.	0-2	X 1.3
Border	Abrupt ending of pigment pattern at the periphery in 0-8 segments.	0-8	X 0.1
Color	Presence of up to six colors (white, red, light-brown, dark-brown, blue-gray, black).	1-6	X 0.5
Differential structures	Presence of network, structureless or homogeneous areas, streaks, dots, and globules.	1-5	X 0.5
Formula for calculating TDS:			
TDS = [(A score x 1.3) + (B score x 0.1) + (C score x 0.5) + (D score x 0.5)]			

The lesion classification is made according to the value of TDS obtained: TDS values less than 4.75 indicates a benign melanocytic lesion, values between 4.8 and 5.45 indicate a suspicious lesion and values greater than 5.45 are highly suspicious for melanoma.

The 7-point checklist is other well-known algorithm, proposed by Argenziano *et al.* in 1998 [7]. This method takes into account 7 different criteria, selected for their frequent association with melanoma. They are divided into "major" and "minor" criteria, and a lesion with score of 3 or more is classified as melanoma (see table 2).

Table 2 – The 7-point checklist criterion.

7-Point Checklist Criteria	Score
Major Criteria	
Atypical pigment network	2
Blue-whitish veil	2
Atypical vascular pattern	2
Minor Criteria	
Irregular streaks	1
Irregular pigmentation	1
Irregular dots/globules	1
Regression structures	1

Several automated systems based on this and others diagnostic algorithms have been proposed during the last years, some of them showing good results. Some of these systems and their specifications are listed in table 2.

A recent study compared the diagnosis accuracy of three commercial systems currently on the market, and concluded that they all tend to classify suspicious melanocytic lesions as melanomas [8], which clearly decrease the clinical application of these models. Thus, it is crucial to continue investigating new systems of diagnosis, being this the main motivation for conducting this thesis.

Table 3 – Some of the recent proposed automatic methods for analyzing dermoscopy images.

Source	*Year*	*Segmentation Method*	*Feature Extraction*	*Classifier*	*SE*[1]	*SP*[2]	*Comments*
[9]	2001	Thresholding + Color Clustering	122 parameters	K-Nearest Neighbors	73%	89%	Feature selection based on ABCD rule.
[10]	2002	Thresholding	48 parameters	Artificial Neural Networks	94%	94%	Features grouped into 4 categories (geometry, color, texture and islands of color).
[11]	2004	Not reported	64 parameters	Linear Regression	82%	87%	-
[4]	2006	Region Growing	Atypical pigment network and atypical vascular pattern	-	-	-	There's no diagnostic, just the detection of these features based on the 7-point checklist method.
[3]	2007	Region Growing	437 parameters	Support Vector Machines	92%	93%	11 features of shape, 354 of color, and 72 of texture.
[12]	2008	Obtained manually with supervision	Blue-whitish veil	Decision Trees	69%	90%	There's no diagnostic, just the detection of this feature based on the 7-point checklist method.
[13]	2008	Clustering + Region Growing	428 parameters	Artificial Neural Networks	86%	86%	Feature selection based on ABCD rule.

[1] Sensibility
[2] Specificity

2. Image Data set

It was used a set of 68 digital dermoscopic images in RGB format provided by the Hospital Pedro Hispano and Faculty of Science, University of Porto, with a typical resolution ranging from 640x481 pixels to 768x577 pixels.

Since we had no control over the image acquisition, the images that satisfied at least one of the following criteria were omitted: the lesion is not fully contained within the image, the presence of too much hair, and poor contrast between the lesion and surrounding skin. This selection process was essential to ensure an effective segmentation and feature extraction. After segmentation 5 more images were omitted to ensure reliable feature extraction. A subset of 44 images was obtained, in which 4 were classified as melanomas and 7 as suspicious lesions by a specialist.

3. Pre-Processing

Before extracting meaningful information from the images, it was necessary to apply some pre-processing procedures:

1) Conversion to grayscale image: Choosing only one of the RGB channels of the images clearly facilitated the implementation of several steps in the system, especially the segmentation and extraction of asymmetry. It was chosen the channel corresponding to the blue color, since it's the RGB component that allows better lesion discrimination [14].

2) Dark corners removal: Due to the characteristics of dermoscopy images used in this study, the 4 dark corners of the images had to be removed through the application of a mask to all images of the dataset.

3) Filtering: In order to remove some artifacts, the images were filtered through a median filter with a 5x5 rectangular window. This step is particularly important for the segmentation result, since its application is very effective in eliminating small structures like thin hairs and isolating small islands of pixels like air bubbles (figure 1).

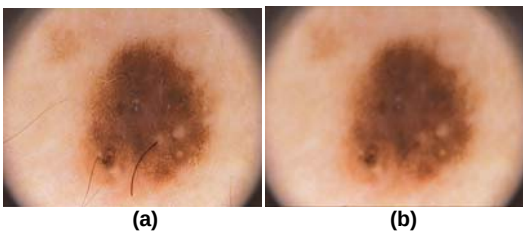

(a) **(b)**

Figure 1 - Original image (**a**) and result after median filtering (**b**).

4. Segmentation

A correct separation of a skin lesion from the remaining surrounding skin plays a key role in the effectiveness of any image automated diagnosis system. Histograms of dermoscopy images are often bimodal, i.e. they usually have 2 peaks corresponding to the area of the lesion and surrounding skin. Thus, it is considered a good threshold the valley between the two representative peaks.

Unfortunately, not all dermoscopic images have a histogram with a clear bimodal distribution. To overcome some difficulties related with this problem, the segmentation method proposed in this paper works as follows:

1) Mean filtering: Its application consists in replacing each pixel value in the image for the arithmetic mean value of its neighbors. Thus its application will reduce the intensity variation between nearby pixels, thus eliminating several local maxima and minima in the histogram with no significant interest.

2) Determination of the representative local maximums: All the local maximums of the histogram are calculated and sorted according to the number of pixels belonging to each value of intensity. Since we want to find the local maximums that represents the two regions of interest (i.e. the region of the lesion and surrounding skin), taking as starting point the two local maxima of the histogram with the largest number of pixels, the following conditions must be verified simultaneously:

$$minimum\,\{I_1, I_2\} < H \quad (1)$$

$$|I_1 - I_2| > \Delta \ , \quad (2)$$

where I_1 and I_2 are the intensity values that corresponds to the two considered local maximums. For condition (1) was chosen H=170, which ensures that the threshold does not corresponds to an area of relatively high intensity, as the lesions usually have a dark color. This is especially important when we have large areas of the image that reflects light with a very high intensity. For condition (2) was chosen Δ=30, which ensures that the two local maximums doesn't belong to the same mode.

If both conditions are not met, the local maximum with a smaller number of pixels is replaced by the next local maximum with a higher number of pixels. This procedure is repeated until both conditions are met.

3) Threshold value: here we want to find the value of intensity that represents the intensity of the pixels near the border of the lesion. One of the most recurrent problems in this step is the existence of several local minimums in the area between the two representative local maximums. We start for finding all local minimums in this range, being the threshold chosen by the following criteria:

i) If only a local minimum is detected in the interval between the two representative peaks, its intensity will be the threshold value.

ii) If exists more than one local minima in the interval between the two peaks, will be chosen the minima that has a much lower number of pixels when compared to the others. In situations where the number of pixels corresponding to each local minimum does not vary significantly between them, the threshold will be the arithmetic mean intensity of these local minimums.

After calculating the threshold, each pixel is classified as active if has the same intensity or is darker than the threshold. To ensure that disconnected areas in this binary image are detected as a whole, a morphological closing operation is applied with a 5x5 rectangular structuring element.

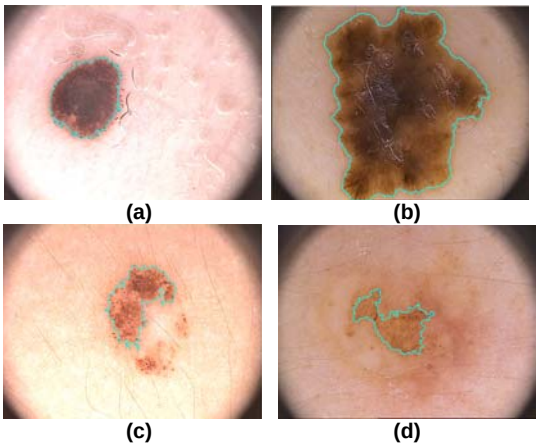

Figure 2 - Examples of successfully (**a**, **b**) and unsuccessful (**c**, **d**) segmentation results.

5. Feature Extraction

5.1 Asymmetry

The asymmetry of a lesion is based on the distribution of colors and shapes of its structures, according to the principal and secondary axes of inertia that intersect at the centroid of the lesion. The centroid $\bar{\mathbf{c}} = (\bar{x},\ \bar{y})$ of a binary image $\mathcal{R}$ can be defined through its geometric moments (see table 4). To find the principal and secondary axes of inertia, we used the central moments μ_{pq} to obtain the angle $\theta_{\mathcal{R}}$ [15]. This angle is used to rotate the image clockwise in order to align the axes of the image with the axes of inertia (figure 3.b).

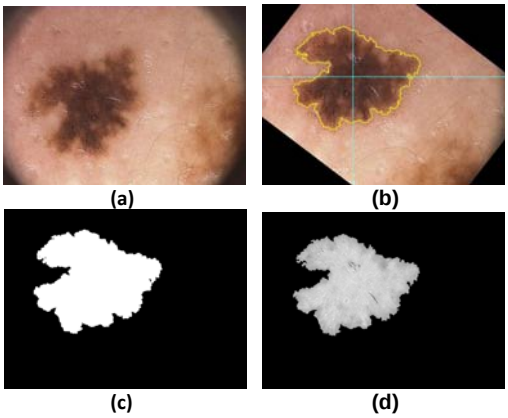

Figure 3 - Rotation of the original image (**a**) in order to align the principal axes (in blue) with the axes of the image (**b**), as well as the obtained mask in binary (**c**) and grayscale (**d**) format.

The symmetry of the lesion as to be analyzed according to its geometry and color, so two types of masks were considered: a binary mask (figure 3.c) and a grayscale mask (figure 3.d). For each of these masks, the image was hypothetically folded along each principal axis, and the difference of the overlap was calculated. The parameters A_x and A_y represents the sum of intensity differences between each overlaid pixel according to the principal axis *x* and *y*, respectively (table 4).

Two asymmetry ratios were considered for each type of mask [3], where *A* represents the area of the lesion for the binary case and the sum all pixels intensities belonging to the lesion for the grayscale case.

Table 4 – Parameters used in the extraction of asymmetry.

Geometric Moment m_{pq}	$m_{pq} = \sum_{(u,v)\in\mathcal{R}} u^p\, v^q$	**Rotation Angle** $\theta_{\mathcal{R}}$	$\theta_{\mathcal{R}} = \frac{1}{2}\tan^{-1}\left(\frac{2\cdot\mu_{11}(\mathcal{R})}{\mu_{20}(\mathcal{R}) - \mu_{02}(\mathcal{R})}\right)$
Centroid $\bar{c} = (\bar{x}, \bar{y})$	$\bar{x} = \frac{m_{10}(\mathcal{R})}{m_{00}(\mathcal{R})} \quad \bar{y} = \frac{m_{01}(\mathcal{R})}{m_{00}(\mathcal{R})}$	**Asymmetry Ratios**	$A_1 = \frac{\min(A_x, A_y)}{A} \times 100$
Central Moment μ_{pq}	$\mu_{pq} = \sum_{(u,v)\in\mathcal{R}} (u-\bar{x})^p \cdot (v-\bar{y})^q$		$A_2 = \frac{A_x + A_y}{A} \times 100$

5.2 Border

The main goal of this feature is to find abrupt ending of pigment pattern at the periphery of the lesion. So we defined two regions, one inside and other outside the lesion. For this purpose, we start by applying a Euclidian Distance Transform (EDT) to the border mask of the lesion obtained in the segmentation stage.

The outer peripheral region is bounded by two contour lines of the image resulting from the EDT image, regions corresponding to areas $1.1 \times A$ and $1.3 \times A$, where A is the area of the lesion. The same procedure is applied for calculating the inner peripheral region, while in this case are considered regions with areas $0.7 \times A$ and $0.9 \times A$. Note that peripheral areas immediately adjacent to the border with an area of 10% of the injured area are omitted, in order to protect the extraction of this feature from errors related with the segmentation process [3].

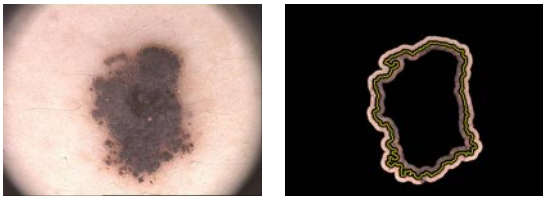

(a) **(b)**

Figure 4 - Original image (**a**) and respective border mask (in yellow), outer peripheral region and inner peripheral region (**b**).

According to the ABCD rule, the lesion is visually divided into eight equal segments, and each one is screened for the presence of abrupt cut-off in the pigment pattern. Therefore we applied a set of 8 masks to the peripheral region mask obtained previously in order to divide the lesion in 8 equal segments. The following ratios are proposed to quantify this feature:

Let be E_i and I_i an image in RGB format which represents the outer and inner peripheral region in channel *i*, respectively, where $i = 1, \dots, 3$. The mean ratio R_m and standard deviation ratio R_d are given by:

$$R_m = min\left(\frac{\bar{x}(E_i)}{\bar{x}(I_i)}, \frac{\bar{x}(I_i)}{\bar{x}(E_i)}\right) \quad (3)$$

$$R_d = min\left(\frac{s(E_i)}{s(I_i)}, \frac{s(I_i)}{s(E_i)}\right) \quad (4)$$

where $\bar{x}$ e s represents the mean and standard deviation. Basically, R_m quantifies if exists a well marked transition between the peripheral regions, while R_d quantifies the irregularity of the lesion in its boundary region.

5.3 Color

The purpose of this feature is to find the six colors proposed by the ABCD rule (black, white, blue-gray, red, light brown and dark brown). To find these colors we will use the distance of each pixel to the color we want to detect.

Table 4 – Detected colors and respective RGB codes.

Black	**White**	**Blue-gray**
(0,0,0)	(255,255,255)	(150,125,150)
(10,10,10)	(245,245,245)	(125,125,150)
(20,20,20)	(235,235,235)	(100,100,125)
(30,30,30)	(225,225,225)	(100,125,150)
(50,40,40)	(215,215,215)	(50,100,150)
(50,50,50)	(205,205,205)	(0,100,150)
Red	**Light Brown**	**Dark Brown**
(255,0,0)	(200,150,100)	(150,100,100)
(255,50,50)	(200, 100, 0)	(125,75,75)
(200,0,0)	(200,100,50)	(100,50,50)
(200,50,50)	(150,100,50)	(100,50,0)
(150,0,0)	(150,100,0)	(100,0,0)
(150,50,50)	(150,50,0)	(50,0,0)

Note that was chosen 6 RGB codes for each color we want to detect (table 4), in order to give flexibility to the algorithm. These codes were chosen as follow: 1) the RGB code that represents the color is chosen as starting point and is used as reference; 2) five more colors were chosen through color combinations that return colors related to the reference code. The choice of these combinations was based purely on experimental results, since there was no possibility to collect data from experts that help the algorithm to learn the colors to detect, and no literature was found that documented this information.

The distance between the referred RGB codes and the value of each pixel is calculated through the sum of the difference in each color channel. A pixel is considered to belong to a particular reference color if the distance between them is less than a predetermined threshold, in order to allow small variations:

Let bet $I(x, y)$ a pixel from the image I in RGB format and I' a reference color. The distance between I and I' is given by:

$$d(x, y) = \sum_{k=1}^{3} \left| I^k(x, y) - I'^k \right| \quad (5)$$

The distance chosen for the threshold was 25, value that was experimentally estimated. The number of pixels that belongs to each group of colors was calculated, and the color is considered present in the lesion if the number of pixels found in that specific group represents at least 0.1% of the lesion area. The number of detected colors represents the color score, as described by the ABCD rule.

5.4 Differential Structures

This feature is intended to detect 5 types of differential structures that usually are associated with the development of melanomas: pigment network, homogeneous areas or without structures, streaks, dots and globules. The approach chosen to extract this feature was based on a methodology developed by Betta et al. [4] with the aim of analyzing the atypical pigmented network (7-Point checklist criteria). Several changes to this methodology were made in order to adapt it to the feature under study. The structure of the algorithm can be seen in figure 5.

Texture Analysis

The texture is analyzed through the entropy of the image. Entropy is a statistical randomness measure of the pixels intensity in an image. An area with high entropy corresponds to regions of the image with relatively high intensity variability of the pixels.

To create the entropy mask, the entropy of each pixel was calculated through a sliding window process, and the pixels were considered active if its value were at least $\frac{2}{3}$ of the maximum of entropy founded in the image (see figure 6).

Structural Analysis

The purpose of this step of the algorithm is to detect local discontinuities in the image. A median filter is applied considering a fairly large neighborhood, which will soften the image and consequently lead to the elimination of the majority of the discontinuities.

The filtered image and the original image are subtracted in order to obtain an intensity differences mask, for which all pixels with intensity greater than 10 are considered a local discontinuity.

The differential structures mask is then obtained through element by element matrix multiplication of the masks obtained by texture and structural analysis (see figure 6).

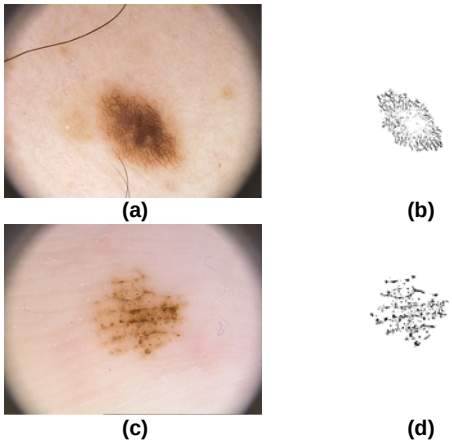

Figure 6 - Examples of differential structures masks obtained.

Let be I a grayscale image. Being M_B the differential structures of image I in binary format, and M_C the group of pixels that represents the differential structures of I, the ratio of area R_a and the intensity standard deviation R_i are given by:

$$R_a = \frac{A_B}{A_L} \times 100 \tag{6}$$

$$R_i = s\,(M_C), \tag{7}$$

where A_B represents the are of M_B, A_L the area of the lesion and s the standard deviation. Since we don't detect separately each one of the five structures referred in the ABCD rule, these two indicators are responsible for quantifying its presence. A high value of R_a is obtained when this structures occupy large areas, while a high R_i indicates significant intensity variability between them, being likely to obtain a large R_i when several differential structures are detected.

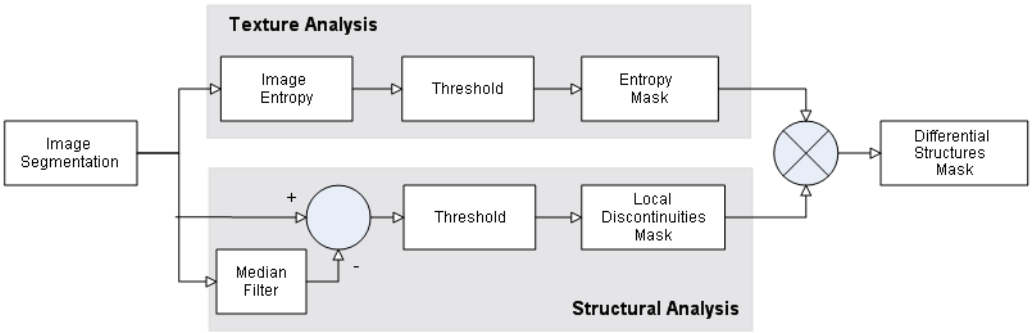

Figure 5 – Block diagram for the extraction of differential structures.

6. Classification Model

The proposed system can be divided into 3 main blocks:

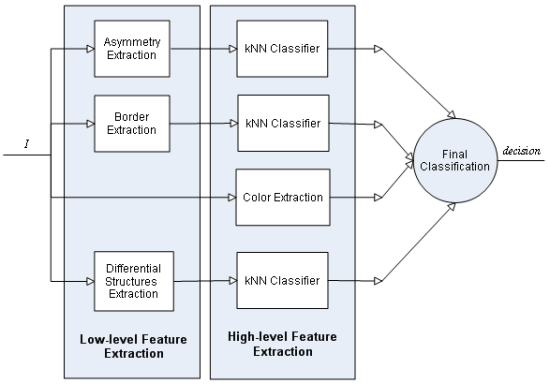

Figure 6 - Block diagram of the proposed classification model.

1) Low-level features extraction: The parameters that quantify the features previously described are extracted. Note that all algorithms responsible for feature extraction (except for the color feature) do not classify the injury as the ABCD rule scoring system, i.e. the range of values are not similar, and so their outputs are called *low-level features*.

2) High-level features extraction: For the three features with a different score format from ABCD rule, the observation vectors are classified through a k-Nearest Neighbor (kNN) classifier. The parameters extracted in the previous steps are used in the classification process, as well as a classification by a specialist according to the ABCD rule for each feature. Hence, a score that's within the range of values proposed by ABCD rule is obtained (*high-level features*).

3) Final classification: Three classifiers were considered: a kNN classifier, which takes as input the ABCD scores obtained in the previous steps; a Support Vector Machines (SVM) classifier, which uses an input similar to the previous classifier; and a thresholding method, which takes as input a linear combination of the ABCD parameters designated TDS (see table 1). The final decision will classify the lesion as suspected or not suspected of being a melanoma. In this final classification is used another classification by a specialist, who classified each image as suspected or not suspected of being a melanoma.

7. Results

7.1 Segmentation

All images were segmented and compared with manual segmentation performed by a specialist for the same data set. The quantification of the discrepancy between automatic and manual segmentation was done using the Hammoude metric [14]:

$$d_H = \frac{\#(X \cup Y) - \#(X \cap Y)}{\#(X \cup Y)} \qquad (7)$$

where X and Y are the active pixels of two binary images. The Hammoude metric take values between 0 and 1, where 0 corresponds to a perfect match between images and 1 when they are completely dissimilar. An acceptable mean and variance values of the Hammoude metric were obtained ($\bar{x} = 0.19$ and $s^2 = 0.024$) when compared with previous studies [14] in which, however, no images were omitted before segmentation by pre-selection criterion.

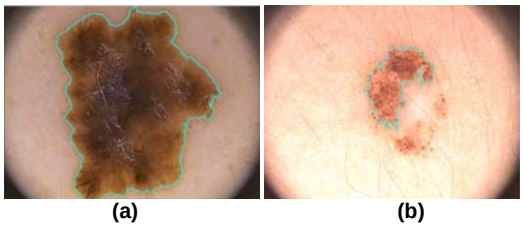

(a) **(b)**

Figure 6 – Examples of successful (**a**) and unsuccessful (**b**) segmentations[3].

7.2 Feature Extraction

To analyze the performance of the kNN classifier for each feature classification, confusion matrices, error probabilities (P_e), and the frequency of each (P_i) class were calculated.

Table 5 – Confusion matrix and P_e for asymmetry classification.

		kNN Classification			P_i
		0	1	2	
Specialist Classification	0	75%	21%	4%	55%
	1	40%	33%	27%	34%
	2	0%	20%	80%	11%
P_e		39%			

The asymmetry of a lesion is classified into 3 classes, as suggested by the ABCD rule. The best classification for asymmetry was obtained for k=3 (table 5). Despite the high error probability of 39%, it was found that the algorithm correctly classifies

[3] Hammoude distances: $d_H^{(a)} = 0.10$ and $d_H^{(b)} = 0.58$.

75% and 80% of the images completely symmetric and asymmetric in both principal axes. The main difficulty seems to be in discriminating the images asymmetric in only one principal axis, which can be a starting point to improve this algorithm.

Table 6 – Confusion matrix and P_e for border classification.

		kNN Classification								
		0	1	2	3	4	5	6	7	8
Specialist Classification	0	26 %	47 %	15 %	12 %	0 %	0 %	0 %	0 %	0 %
	1	-	-	-	-	-	-	-	-	-
	2	38 %	50 %	13 %	0 %	0 %	0 %	0 %	0 %	0 %
	3	-	-	-	-	-	-	-	-	-
	4	-	-	-	-	-	-	-	-	-
	5	-	-	-	-	-	-	-	-	-
	6	-	-	-	-	-	-	-	-	-
	7	-	-	-	-	-	-	-	-	-
	8	0 %	50 %	50 %	0 %	0 %	0 %	0 %	0 %	0 %
P_e		77%								

The border classification is a nine class problem, and probably because of the small size of the data set only 3 of these classes have representatives in the training set. So the classification by the specialist was divided in just two classes: the presence or absence of abrupt cut-off. The images were firstly divided into 8 equal segments, and each segment was classified by a kNN classifier, being awarded 1 point if the segment is classified as belonging to the class where a cut-off exists and 0 points otherwise. The sum of all segments scores represents the border score, which can vary between 0 and 8, as described by ABCD rule.

Due to all these limitations, the high error probability was already expected (table 6), and so its essential to test this algorithm with an appropriately classified data set in order to measure its true potential in detecting the border cut-off.

Table 7 – Confusion matrix and P_e for color classification.

		Algorithm Classification						P_i
		1	2	3	4	5	6	
Specialist Classification	1	63%	32%	5%	0%	0%	0%	45%
	2	15%	65%	20%	0%	0%	0%	48%
	3	67%	33%	0%	0%	0%	0%	7%
	4	-	-	-	-	-	-	0%
	5	-	-	-	-	-	-	0%
	6	-	-	-	-	-	-	0%
P_e		40%						

Looking at table 7, we can see that the effectiveness of the algorithm can not be analyzed for all possible classes, since the lesions in the data set only have a maximum of 3 colors for both types of classification. A high error probability is also obtained for the algorithm responsible for color extraction (P_e=40%), however, two of the three classes in the data set were correctly detected in the majority of the cases, with 63% and 65%. Also note that most of the misclassified cases only differ from specialist classification by the presence or absence of one color.

Table 8 – Confusion matrix and P_e for differential structures classification.

		kNN Classification					P_i
		1	2	3	4	5	
Specialist Classification	1	46%	54%	0%	0%	0%	30%
	2	12%	85%	4%	0%	0%	59%
	3	0%	60%	40%	0%	0%	11%
	4	-	-	-	-	-	0%
	5	-	-	-	-	-	0%
P_e		32%					

According to ABCD rule, one point is given for each structure detected, and the differential structures score corresponds to the sum of the scores of the 5 considered structures. However, the proposed algorithm does not make an independent detection of each of these structures, but quantifies its presence and variability, which could contribute to the error probability of 32%.

The majority of the cases for classes 1 and 3 are not correctly classified, probably because the best kNN classification was obtained for k=5, which can be a problem due to the high frequency of the class 2 and the high number of nearest neighbors considered.

7.3 Final Classification

As already mentioned, the number of suspicious lesions in the dataset was very small, so the data of these cases were tripled in order to ensure a similar frequency in both classes. The results obtained for the three different classifiers are resumed in table 9.

Table 9 – Summary of the final classification results.

Input	Classifier	P_e	*SE*	*SP*
ABCD features scores	kNN	34%	**82%**	61%
ABCD features scores	SVM	45%	36%	61%
TDS	Thresholding	**30%**	73%	**70%**

The best classification seems to be given by the thresholding method. In this method the threshold that minimizes the error probability of the training set classification is chosen. This classification has

the lower error probability and achieves the best sensibility (SE) and specificity (SP) values. Note that this method uses the PDT calculated from the ABCD features scores obtained, and thus is influenced by the weight that each class represents in the final score of the lesion, as suggested by the ABCD rule.

However, the best sensibility is achieved by the kNN classifier, which is more effective in the detection of suspicious cases among the cases that were classified as suspicious by the specialist.

8. Conclusions and Further Work

In this work was developed a system for automatic diagnosis of skin lesions based on the ABCD rule, by which the best classification was obtained by a thresholding method, with *SE*=73%, *SP*=70% and P_e=30%.

From an initial set of 68 images, 44 were used to test this model after a selection step. Among these 44 images only 4 were classified as melanoma and 7 as suspicious lesions by a specialist, which certainly limits the classification process of the implemented model. So a database of higher dimensions and properly classified should be used in future works with this tool.

The images used in the model were manually segmented by a specialist and automatic segmented by a proposed method based on histogram analysis. The results showed a satisfactory segmentation of the lesions, but routines to eliminate several artifacts such as thick hairs must be developed.

A set of 4 high-level features based on the ABCD rule was chosen to classify the images. Despite the overall error probability achieved with the extraction of these features, encouraging results were obtained in some of them. In particular, the algorithm responsible for asymmetry extraction achieved 75% and 80% of correct classification for lesions completely symmetric and asymmetric in both principal axes, respectively. The color and differential structures extraction algorithms correctly classified the majority of the cases, and the misclassified lesions belong to nearby classes in most cases. The worst results were obtained for border extraction, with an error probability of 77%. This value is probably due to the fact that this feature is evaluated in nine different classes, which allied to the small size of the database greatly affected the results.

In conclusion, some steps of the segmentation and feature extraction of the automatic system proposed in this work must be improved in order to make this model an effective tool in the diagnosis of skin lesions by dermoscopy images.

9. References

1. Site da Liga Portuguesa Contra o Cancro. [Online] http://www.ligacontracancro.pt/.
2. *Parameterization of Dermoscopic Findings for the Internet-based Melanoma Screening System.* H. Iyatomi, H. Oka, M. E. Celebi, M. Tanaka, and K. Ogawa. Proc. IEEE Symposium on Computational Intelligence in Image, 2007, pp. 189-193.
3. *A methodological approach to the classification of dermoscopy images.* M.E. Celebi, H.A. Kingravi and B. Uddin. Computerized Medical Imaging and Graphics, 2007, Vol. 31, pp. 362-373.
4. *Dermoscopic image-analysis system: estimation of atypical pigment network and atypical vascular pattern.* G. Betta, G. Di Leo, G. Fabbrocini, A. Paolillo, P. Sommella. IEEE International Workshop on Medical Measurement and Applications, 2006, pp. 63-67.
5. *ABCD rule of dermatoscopy: a new practical method for early recognition of malignant melanoma.* Stolz W, Riemann A, Cognetta AB. Eur J Dermatol, 1994, Vol. 4, pp. 521-527.
6. Dermoscopy.org. [Online] http://www.dermoscopy.org/.
7. *Epiluminescence microscopy for the diagnosis of doubtful melanocytic skin lesions. Comparison of the ABCD rule of dermatoscopy and a new 7-point checklist based on pattern analysis.* Argenziano G, Fabbrocini G et al. Arch Dermatol., 1998, Vol. 134, pp. 1563-1570.
8. *Current and emerging technologies in melanoma diagnosis: the state of the art.* E. Psaty, A. Halpern. Clin Dermatol, 2009, Vol. 27, pp. 35-45.
9. *Automated melanoma recognition.* H. Ganster, A. Pinz, et al. IEEE transaction on Medical Imaging, 2001, Vol. 20. pp. 233-239.
10. *Automated diagnosis of pigmented skin lesions.* P. Rubegni, G. Cevenini, M. Burroni, R. Perotti, G. Dell'Eva, P. Sbano, et al. International Journal of Cancer, 2002, Vol. 101, pp. 576-580.
11. *Digital image analysis for diagnosis of cutaneous melanoma. development of a highly effective computer algorithm based on analysis of 837 melanocytic lesions* A. Blum, H. Luedtke, U. Ellwanger, R. Schwabe, G. Rassner, C. Garbe. Br J Dermatol, 2004, Vol. 151, pp. 1229-1238.
12. *Automatic Detection of Blue-White Veil and Related Structures in Dermoscopy Images.* M. E. Celebi, H. Iyatomi, W. V. Stoecker, R. H. Moss, H. S. Rabinovitz, G. Argenziano, and H. P. Soyer. Computerized Medical, 2008, Vol. 32, pp. 670-677.
13. *An Improved Internet-Based Melanoma Screening System with Dermatologist-like Tumor Area Extraction Algorithm.* H. Iyatomi, H. Oka, M. E. Celebi, M. Hashimoto, M. Hagiwara, M. Tanaka, and K. Ogawa. Computerized Medical Imaging and Graphics, 2008, Vol. 32, pp. 566-579.
14. *Comparison of segmentation methods for automatic diagnosis of dermoscopy images.* **T.**

Mendonca, A. Marcal, A. Vieira A, J. Nascimento, M. Silveira, J. Marques, J. Rozeira. Proceedings of the 29th IEEE EMBS Annual International Conference, 2007, Vol. 1, pp. 6572-6575.
15. *Digital image processing: an algorithmic introduction using Java.* Burger, Wilhelm. Springer, 2008.
16. *Early diagnosis of malignant melanoma by surface microscopy.* H.P.Soyer, J.Smolle, H.Kerl and H.Stettnre. Lancet, 1987, Vol. 2.
17. *Current and emerging technologies in melanoma diagnosis: the state of the art.* E. Psaty, A. Halpern. 1, Vol. 27, pp. 35-45.
18. *Diagnostic accuracy of dermoscopy.* H Kittler, H Pehamberger, K Wolff, and M Binder. The Lancet Oncology, 2002, Vol. 3.
19. *Computer image analysis in the diagnosis of melanoma.* A. Green, N. Martin, J. Pfitzner, M. O'Rourke, and N. Knight. J. Amer. Acad. Dermatol, 1994, Vol. 31, pp. 958-964.
20. *In vivo epiluminescence microscopy of pigmented skin lesions.* Pehamberger H, Steiner A, Wolff K. J Am Acad Dermatol., 1987, Vol. 17, pp. 571-583.
21 *A possible new tool for clinical diagnosis of melanoma: The computer.* Cascinelli N, Ferrario M, Tonelli T, Leo E. J Am Acad Dermatol, 1987, Vol. 16, pp. 361-367.
22. *Parameterization of Dermoscopic Findings for the Internet-based Melanoma Screening System.* H. Iyatomi, H. Oka, M. E. Celebi, M. Tanaka, and K. Ogawa. Proc. IEEE Symposium on Computational Intelligence in Image, 2007, pp. 189-193.
23. *Epiluminescence microscopy: criteria of cutaneous melanoma progression.* Argenziano G, Fabbrocini G, Carli P, et al. s.l.Â : J Am Acad Dermatol, 1997, Vol. 37. 68-74.
24. *Digital Image Processing using Matlab.* R. C. Gonzalez, R. E. Woods, S. L. Eddins. Prentice Hall, 2004.
25. Wikipédia, a enciclopédia livre. [Online] http://pt.wikipedia.org.